Available online at www.sciencedirect.com

ScienceDirect

Advances in Space Research 55 (2015) 2114–2123

ADVANCES IN SPACE RESEARCH (a COSPAR publication)

www.elsevier.com/locate/asr

The IONORT-ISP-WC system: Inclusion of an electron collision frequency model for the D-layer

Alessandro Settimi *, Marco Pietrella, Michael Pezzopane, Cesidio Bianchi

Istituto Nazionale di Geofisica e Vulcanologia, Via di Vigna Murata 605, I-00143 Rome, Italy

Received 5 March 2014; received in revised form 24 July 2014; accepted 31 July 2014
Available online 9 August 2014

Abstract

The IONORT-ISP system (IONOspheric Ray-Tracing – IRI-SIRMUP-PROFILES) was recently developed and tested by comparing the measured oblique ionograms over the radio link between Rome (41.89°N, 12.48°E), Italy, and Chania (35.51°N, 24.02°E), Greece, with the IONORT-ISP simulated oblique ionograms (Settimi et al., 2013). The present paper describes an upgrade of the system to include: (a) electron-neutral collision have been included by using a collision frequency model that consists of a double exponential profile; (b) the ISP three dimensional (3-D) model of electron density profile grid has been extended down to the altitude of the D-layer; (c) the resolution in latitude and longitude of the ISP 3-D model of electron density profile grid has been increased from 2° × 2° to 1° × 1°. Based on these updates, a new software tool called IONORT-ISP-WC (WC means with collisions) was developed, and a database of 33 IONORT-ISP-WC synthesized oblique ionograms calculated for single (1-hop paths) and multiple (3-hop paths) ionospheric reflections. The IONORT-ISP-WC simulated oblique ionograms were compared with the IONORT-IRI-WC synthesized oblique ionograms, generated by applying IONORT in conjunction with the International Reference Ionosphere (IRI) 3-D electron density grid, and the observed oblique ionograms over the aforementioned radio link. The results obtained show that (1) during daytime, for the lower ionospheric layers, the traces of the synthesized ionograms are cut away at low frequencies because of HF absorption; (2) during night-time, for the higher ionospheric layers, the traces of the simulated ionograms at low frequencies are not cut off (very little HF absorption); (3) the IONORT-ISP-WC MUF values are more accurate than the IONORT-IRI-WC MUF values.

Keywords: Ray-tracing; Electron density; IRI; Assimilative modelling; Oblique ionogram; Electron collision frequency model

1. Introduction

Ionospheric ray-tracing is a technique used to determine the path of a high frequency (HF) radio wave propagating in the ionosphere from a transmitting point to a receiving point.

Over the horizon radar systems, single station location, HF direction finding systems, the management of HF radio communications, and the predictions of operating frequencies, are examples of the main applications of ray-tracing, where a detailed knowledge of radio wave propagation through the ionosphere is needed.

Accurate ray-tracing is usually performed using numerical techniques requiring Haselgrove's equations (Haselgrove, 1955; Haselgrove and Haselgrove, 1960). The propagation of the wave, i.e., the ray path, is described by six differential equations where the parameters of both the position and ray direction need to be integrated simultaneously at each point along the ray path. The integration provides the coordinates reached by the wave vector and its three components, the group time delay of the wave along the path, and other optional quantities such as absorption,

* Corresponding author. Tel.: +39 06 51860719; fax: +39 06 51860397.
E-mail addresses: alessandro.settimi@ingv.it (A. Settimi), marco.pietrella@ingv.it (M. Pietrella), michael.pezzopane@ingv.it (M. Pezzopane), cesidio.bianchi@ingv.it (C. Bianchi).

http://dx.doi.org/10.1016/j.asr.2014.07.040
0273-1177/

polarization, etc. The first ray-tracing algorithms developed in the 1960s (Dudziak, 1961; Lawrence and Posakony, 1961; Croft and Gregory, 1963; Jones, 1966) ran on old mainframes that provided only a numerical output. Since then, many other ray-tracing programs have been developed. For example, Norman and Cannon (1997) developed a two dimensional (2-D) analytic ray-tracing method called SMART for which computer run times are about 10 times faster than those of numerical ray-tracing packages. SMART automatically segments the ionosphere in terms of ground range and it is able to accurately ray-trace through complicated horizontal gradients along the direction of the ray path. Nowadays, the modern ray-tracing procedures (Coleman, 1998; Nickisch, 2008) have been optimized and adapted to over the horizon radar applications using powerful computers and devices for real-time use.

Recently an applicative software tool package named IONORT (IONOspheric Ray-Tracing), able to work both with analytical and numerical electron density models, was developed at the Istituto Nazionale di Geofisica e Vulcanologia (INGV), for calculating a 3-D ray-trace for HF waves propagating in the ionospheric medium (Azzarone et al., 2012).

The validity of IONORT was checked by comparing at different frequencies the time delay of the wave that results from the ray-tracing computation performed by IONORT (t_{calc}), and the time delay of the wave propagating along the oblique virtual path at the speed of light (t_{virt}). It was found that the IONORT ray-tracing algorithm fits nearly perfectly the theory so that the relative error $\Delta t = t_{calc} - t_{virt}$ is only due to the discrete integration step (Bianchi et al., 2011).

Ray-tracing can generally be performed accurately if the 3-D electron density distribution between the transmitter and the receiver is known (Kashcheyev et al., 2012). A comprehensive specification of the ionosphere in terms of electron density, neutral particles-electrons collision frequency, and geomagnetic field is required in order to carry out an accurate ray-tracing. Therefore, when dealing with near real-time applications of ray-tracing, it is of crucial importance to have a realistic ionospheric modelling through 3-D models of ionospheric electron density, which after assimilating measured data calculate an updated 3-D image of the ionosphere (Angling and Khattatov, 2006; Thompson et al., 2006; Fridman et al., 2006, 2009; Decker and McNamara, 2007; McNamara et al., 2007, 2008, 2010, 2011, 2013; Angling and Jackson-Booth, 2011; Shim et al., 2011). More recently, at the INGV, the IRI-SIRMUP-PROFILES (ISP) model, capable of providing a 3-D electron density profile representation of the ionosphere in quasi real time, was developed.

The ISP model has proven very effective in providing reliable electron density profiles under quiet and disturbed geomagnetic conditions in several studies (Pezzopane et al., 2011, 2013). In particular at the solar terminator, the electron densities calculated by the ISP model more accurately represented the real conditions of the ionosphere than electron densities calculated using the climatological IRI-URSI model alone.

Recently IONORT was used in conjunction with two kinds of 3-D electron density grids: one generated by the International Reference Ionosphere (IRI) electron density model; and the other one outputted by the ISP model (Pezzopane et al., 2011) after assimilating autoscaled foF2 and M(3000)F2 data, and real-time vertical electron density profiles from the reference stations of Rome (41.8°N, 12.5°E), Gibilmanna (37.9°N, 14.0°E) in Italy, and Athens (38.0°N, 23.5°E) in Greece.

Synthesized oblique ionograms over the radio link between Rome and Chania (35.51°N, 24.02°E), Greece, were produced by the IONORT-IRI and IONORT-ISP system and compared with the measured oblique ionograms (Settimi et al., 2013). The comparisons carried out both in terms of the ionogram shape and the maximum usable frequency (MUF) characterizing the radio path have shown that the ISP model can more accurately represent real conditions in the ionosphere than the IRI model, and that the ray-tracing results computed by IONORT are reasonably reliable.

The present paper is inspired by the abovementioned Settimi et al. (2013) study. With the aim of extending this study, the IONORT-ISP system was upgraded including a collision frequency model between electrons and neutral particles, consisting of a double exponential profile (Jones and Stephenson, 1975). Moreover, some changes with respect to the previous version of the ISP model were made; the ISP electron density profile grid is also modified starting now with the D-layer (starting point at 65 km) and increasing the resolution in latitude and longitude from $2° \times 2°$ to $1° \times 1°$.

On the basis of these updates, a new software tool package, to which we refer hereafter as IONORT-ISP-WC (WC, means with collisions), was developed and a database of 33 IONORT-ISP-WC synthesized oblique ionograms completed with single (1-hop paths) and multiple (3-hop paths) ionospheric reflections was produced over the same radio link aforementioned. Some representative examples of the IONORT-ISP-WC synthesized oblique ionograms are shown and discussed in terms of comparison with the IONORT-IRI-WC synthesized oblique ionograms and the observed oblique ionograms. Section 2 describes the electron collision frequency model for the D-layer included in the IONORT-ISP system. We describe our results in Section 3. Concluding remarks and possible future developments are summarized in Section 4.

2. Description of the electron collision frequency model for the D-layer

Collisions of free electrons with neutrals, heavy ions, or other electrons are important causes of various macroscopic phenomena. Electron collisions play an important role in the absorption of radio waves at lower altitudes

(D-layer) (Settimi et al., 2014). Using an appropriate theory (Davies, 1990) it is possible to deduce the electron collision frequency from radio wave propagation data. According to Budden (1965), for a detailed quantitative interpretation of some experiments it is necessary to apply the generalized theory (Sen and Wyller, 1960), while for most practical radio propagation problems, the classical theory (Appleton and Chapman, 1932) is adequate, especially when appropriate values are available for the effective electron collision frequency.

There is a large number of electron collision frequency models, for example constant collision frequency, and exponential and tabular profiles (see references in Jones and Stephenson, 1975). It should be noted that if users want to implement other collision frequency models, they must write a subroutine to calculate the normalized frequency $Z = \nu/2\pi f$ (where ν is the collision frequency between electrons and neutral air molecules, and f is the transmitted wave frequency) and its gradients ($\partial Z/\partial r$, $\partial Z/\partial\theta$, $\partial Z/\partial\varphi$) as a function of position within spherical polar coordinates (r, θ, φ) referring to a system of computational coordinates (which is not necessarily the same as geographic coordinates).

The current version of the IONORT-ISP-WC system includes a collision frequency model between electrons and neutrals for the D-layer that consists of a double exponential profile (Jones and Stephenson, 1975)

$$\nu(h) = \nu_1 e^{-a_1(h-h_1)} + \nu_2 e^{-a_2(h-h_2)}, \quad (1)$$

where ν is the collision frequency at the height above ground h. The first exponential has the following specifications: collision frequency at height h_1, $\nu_1 = 3.65 \cdot 10^4$ collisions per second; reference height, $h_1 = 100$ km; exponential decrease of ν with height, $a_1 = 0.148$ km^{-1}. The second exponential has the following specifications: collision frequency at height h_2, $\nu_2 = 30$ collisions per second; reference height, $h_2 = 140$ km; exponential decrease of ν with height, $a_2 = 0.0183$ km^{-1}. Fig. 1 shows the trend of the electron collision frequency implemented in the IONORT-ISP-WC system.

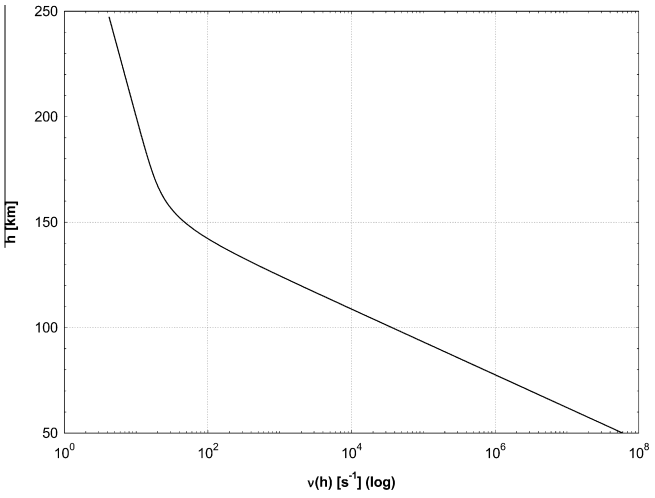

Fig. 1. Semi-logarithmic plot of the electron collision frequency ν, in units of s^{-1}, as a function of height above ground h, in the range 50 – 250 km obtained from Eq. (1).

It should be noted that, in Settimi et al. (2014) paper, simple complex eikonal equations, in quasi-longitudinal (QL) approximation (Rawer, 1976), for calculating the non-deviative absorption coefficient due to the propagation across the D-layer were encoded into a so called COMPLEIK (COMPLex EIKonal) subroutine of the IONORT program. The IONORT program already included the same electron collision frequency model for the D-layer, consisting of the double exponential profile (Jones and Stephenson, 1975). As main outcome of that paper, the simple COMPLEIK algorithm was compared to the more elaborate semi-empirical ICEPAC formula (Stewart, undated). COMPLEIK is just as reliable as ICEPAC, with the advantage of being implemented more directly. Settimi et al. (2014), applying just Eq. (1) (Fig. 1), proved that, the non-deviative absorption profiles corresponding to COMPLEIK are just as reliable as the ICEPAC formula, for all the ordinary and extraordinary rays effectively radio linking Rome and Chania. Instead, the absorption profiles corresponding to the COMPLEIK subroutine lose their reliability just for all the rays that cannot establish the radio link Rome-Chania.

Each synthesized ionogram was computed with or without applying the electron collision frequency model. For the sake of clarity, the synthesized ionograms are generated considering only the ordinary trace and taking into account the geomagnetic field.

For all cases, with the exclusion of those at the solar terminator and during the night, an oblique ionogram computed without applying the electron collision frequency model (1) consists of (e.g., Settimi et al., 2014): (1) a trace for the ionospheric F1-F2 layers at high altitudes ($h > 150$ km); (2) a trace for the E-layer at lower altitude (90 km $< h \leqslant 150$ km). Generally, an ionogram computed applying the electron collision frequency model (1) shows the trace of F1–F2 layers, characterized by a typical absorption coefficient, i.e. $L \leqslant 20$ dB, but does not show the trace of E-layer with a higher absorption coefficient, i.e. $L >> 20$ dB (e.g., McNamara, 1991).

3. Results and discussion

This section discusses some examples of the ray path calculated by means of the proposed IONORT-ISP-WC system and some results obtained by comparing the IONORT-ISP-WC synthesized oblique ionograms with the IONORT-IRI-WC synthesized oblique ionograms and the oblique ionograms measured along the Rome-Chania radio link. The database of the observed oblique ionograms used in this study, is constituted by 33 oblique ionograms recorded over the Rome-Chania radio link in June, July, and October 2011 in the daytime, night-time,

at sunrise, and at sunset during quiet and moderate geomagnetic activity.

The ionograms comprising this database were selected on the criteria of: (a) clarity of trace, which is essential in order to perform a trace shape comparison between measured and synthesized ionograms. In this respect it is worth noting that often the recorded Rome-Chania radio link traces were either noisy or characterized by interference phenomena preventing users from accurately validating the MUF, in addition to not being tagged for polarization; (b) most of the ionograms had to be recorded at specific times for which both the Athens autoscaling, and at least one between the Rome and Gibilmanna autoscalings were available and essentially correct. These "boundary conditions" greatly limited the number of measured oblique ionograms in the test database. The (b) requirement is necessary to guarantee that the assimilation process was properly performed with data from at least two ionospheric stations located close to the two extremities of the radio path. It will be seen in Section 4 that the assimilation of data from only one station at only one extremity of the radio path can cause significant underestimation/overestimation of the real MUF.

Fig. 2 shows four examples of the IONORT's graphical user interface (for a more detailed description of this interface, see Azzarone et al. (2012)).

Each example shows the 2-D (at the bottom) and 3-D (on the right side) ray paths along the Rome-Chania radio link (azimuth angle equal to 121.6°), which falls beyond the validity area of regional ISP model (−10° to 40° in longitude, 30–50° in latitude). The ray paths were calculated taking into account the geomagnetic field, the electron collision frequency model for the D-layer (Eq. (1)), and the electron density profile grid calculated at the epoch 26 June 2011 at 01:00 UT by the global IRI model.

It must be noted that the IONORT-IRI-WC system, with respect to the previous version IONORT-IRI, is now able to provide ray paths also with multiple (3-hop paths) ionospheric reflections, as shown for the two cases depicted at the bottom of Fig. 2.

In all the synthesized ionograms with single or multiple ionospheric reflections (1 – 3 hop paths), even though the

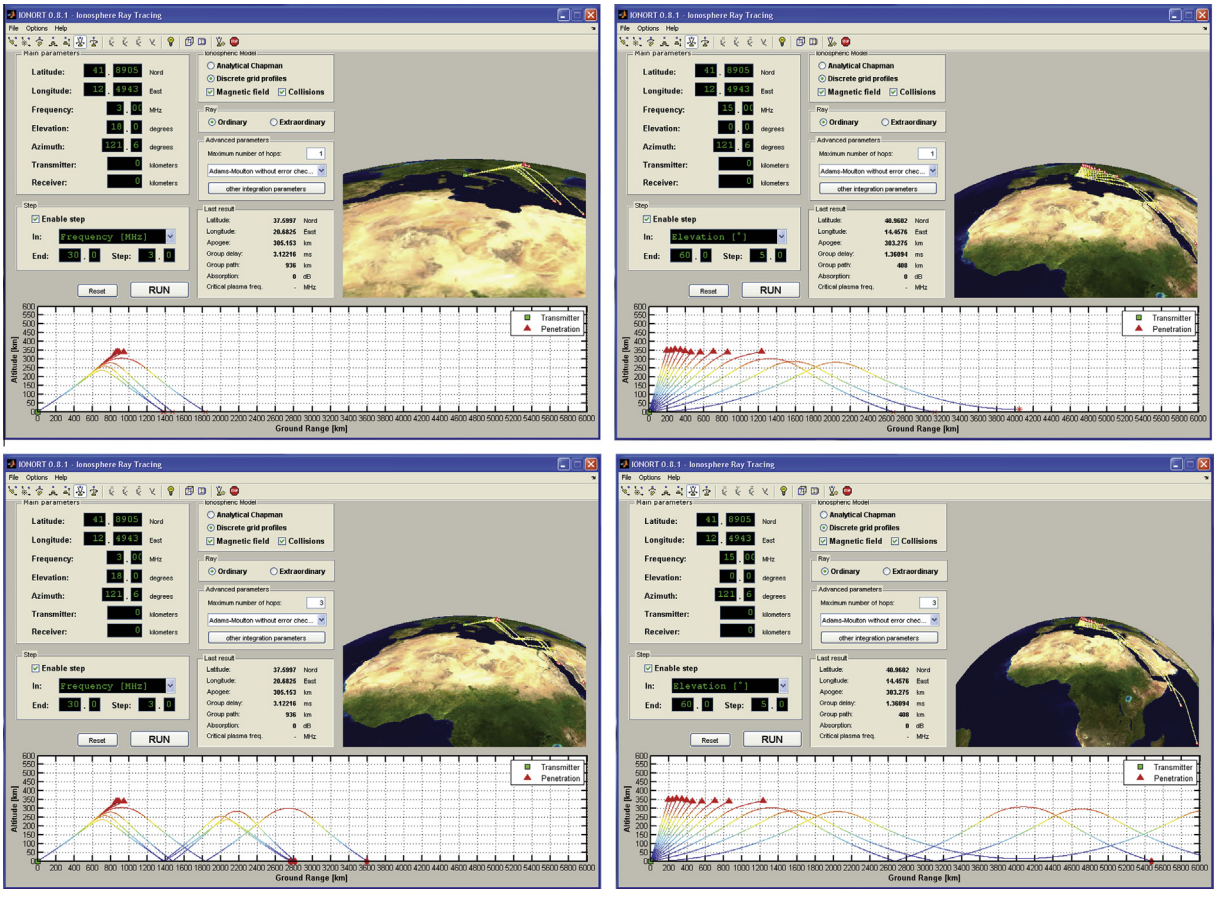

Fig. 2. Graphical user interface of IONORT program. The 2-D and 3-D visualizations of the ray paths are shown at the bottom and right respectively, considering a transmitter point at Rome and an azimuth angle of transmission equal to 121.6° (direction of Chania), on 26 June 2011 at 01:00 UT. To realize the full potential of IONORT, composite simulations, based on the global IRI model, are performed not only inside but also outside the central Mediterranean region, by taking the geomagnetic field and the electron collisions into account, with single or multiple ionospheric reflections (1–3 hop paths): for a fixed elevation angle of 18° with a 3 MHz frequency-step procedure from 3 MHz to 30 MHz; and for a fixed frequency of 15 MHz with a 5° elevation-step procedure from 0° to 60°.

ionosphere is not characterized by large horizontal gradients, a nested loop cycle was iterated with azimuth angles from 121° to 122° of step 0.2°. The elevation angle step was set to 0.2° and the receiver (RX) range accuracy to 0.1% (for a more detailed description of how the parameters, i.e. azimuth, elevation steps and RX range accuracy, are used in the ray-tracing program, we refer the reader to Appendix A of Settimi et al. (2013)).

Fig. 3 shows an example of an oblique ionogram recorded over the Rome-Chania radio link on 07 July 2011 at 15:00 UT (top panel), and its corresponding synthesized ionograms generated by the IONORT-IRI-WC (middle panel) and IONORT-ISP-WC (bottom panel) system. The cases labelled with NC (NC means No Collisions) obtained without including the electron collision frequency model for the D-layer (Eq. (1)) are also shown for a further and more comprehensive comparison.

The case of Fig. 3 shows clearly that the inclusion of the electron collision frequency for the D-layer during daytime has the effect of cutting away the trace of the synthesized ionogram at the low frequencies for the lower ionospheric layer (E region). As expected, both for 1-hop paths and 3-hop paths, the Lowest Observed Frequencies (LOF) calculated not taking into account the collisional model, both in case of IRI and ISP electron density profile grids, are systematically much smaller than those calculated when the collisional model provided by the Eq. (1) is applied. More precisely looking at 1-hop paths, for IRI electron density profile grids (see second panel of Fig. 3), $LOF_E = 4.2$ MHz with NC and $LOF_E = 10.0$ MHz in case of WC, so that a trace long 5.8 MHz is cut off because of absorption; for the higher ionospheric layer (F region) $LOF_F = 5.6$ MHz with NC and $LOF_F = 5.5$ MHz in case of WC, which means that the trace is not cut off. This is also an expected result because at the height of F region the effect of the collisions is less important and therefore the waves propagating at a given frequency do not suffer an important absorption. For ISP electron density profile grids (see third panel of Fig. 3), $LOF_E = 3.1$ MHz with NC and $LOF_E = 9.9$ MHz in case of WC; in this case a trace 6.8 MHz long is missing because of absorption suffered by the wave propagating at the height of E region. Again, at higher heights the effect of the collisions on the propagating waves can be considered negligible because the calculated LOF values are similar being $LOF_F = 9.0$ MHz with NC and $LOF_F = 8.8$ MHz in case of WC.

It must be noted that the MUF values calculated with or without the collisions, in all the cases analyzed show the same value when a given electron density model is applied (IRI or ISP); this is a reasonable result because MUF depends only on the highest frequency reflected by the F2-layer, (foF2), and the secant of the optimum angle at which to broadcast a signal that is to be received at a given distance D, (M(D)F2).

The two cases in Fig. 4 show an example of oblique ionograms recorded over the Rome-Chania radio link on 9 October 2011 at 03:00 UT (at the top, on the left), and

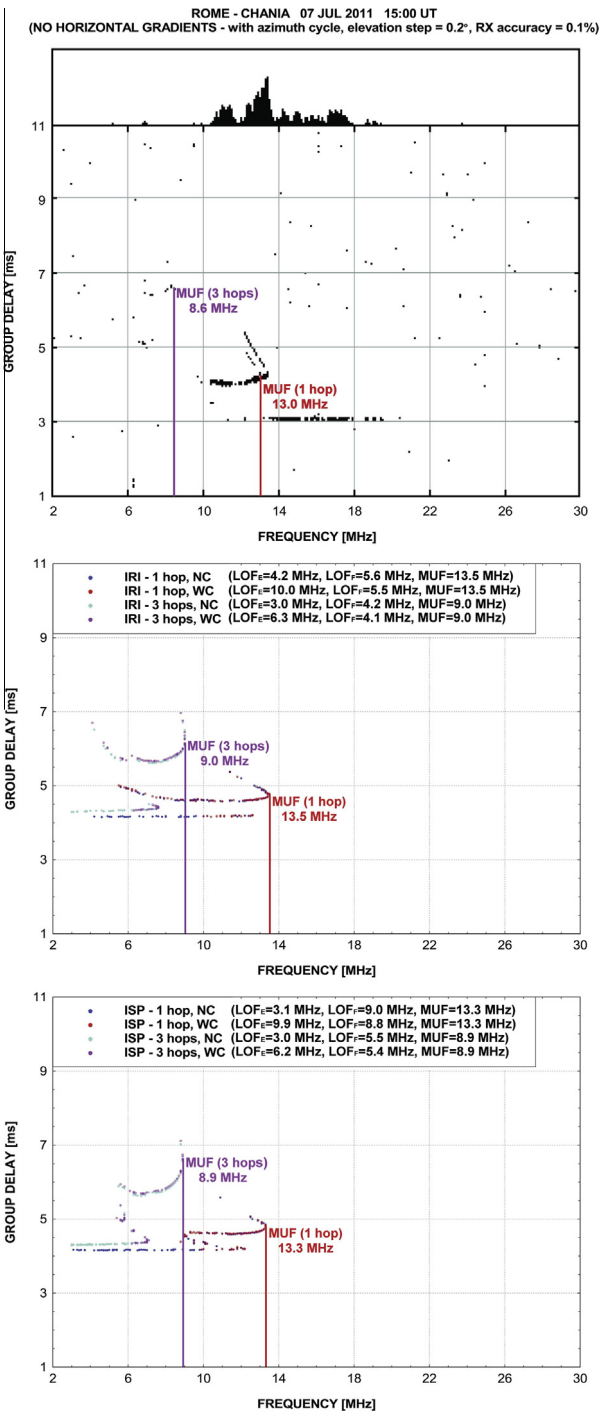

Fig. 3. A comparison between the oblique ionogram recorded over the Rome-Chania radio link on 07 July 2011 at 15:00 UT (top panel), and the corresponding ionograms synthesized by the IONORT-IRI-WC (middle panel) and IONORT-ISP-WC (bottom panel) system. The red and purple vertical lines indicate the MUF values for the 1-hop and 3-hop paths respectively. The LOF values are also indicated for the E and F regions. For the sake of clarity, only the ordinary trace computed taking the geomagnetic field into account is shown. Both with single and multiple ionospheric reflections (1–3 hop paths), a nested loop cycle was iterated with azimuth angles from 121° to 122° of step 0.2°. The elevation angle step was set to 0.2° and the RX range accuracy to 0.1%. The ionograms calculated without applying the collisional model of Eq. (1), labelled with NC are also shown for a further comparison. (For interpretation of the references to colour in this figure legend, the reader is referred to the web version of this article.)

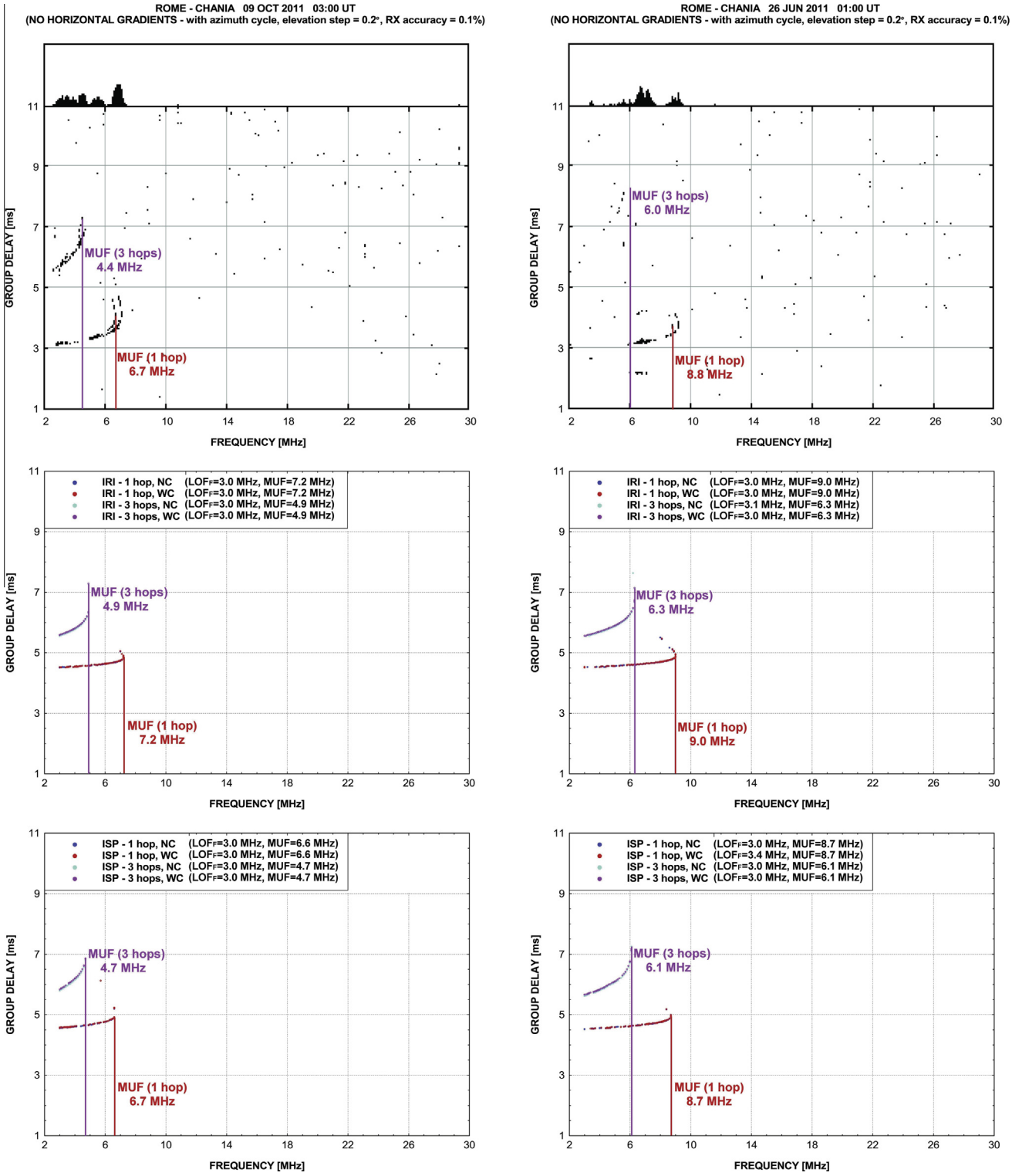

Fig. 4. Same as in Fig. 3. A comparison is shown between the ordinary traces of the oblique ionograms recorded over the Rome-Chania radio link on 09 October 2011 at 03:00 UT (top panel, on the left), and 26 June 2011 at 01:00 UT (top panel, on the right), and the corresponding ionograms synthesized by the IONORT-IRI-WC (middle panels) and IONORT-ISP-WC (bottom panels) system. The ionograms calculated without applying the collisional model of Eq. (1), labelled with NC are also shown for a further comparison.

26 June 2011 at 01:00 UT (at the top, on the right) with their corresponding synthesized ionograms generated by the IONORT-IRI-WC (middle panels) and IONORT-ISP-WC (bottom panels). For a further and more comprehensive comparison, no-collision (NC) cases are also included.

It should be noted that these two examples are relative to ionograms observed during night-time when the

Table 1
The MUF values calculated by the IONORT-IRI-WC system (column A), the MUF values calculated by the IONORT-ISP-WC system (column B), the measured MUF values (column C), the differences IONORT-IRI-WC MUF – measured MUF (Δ_{IRI}, column D) and IONORT-ISP-WC MUF – measured MUF (Δ_{ISP}, column E) are shown for all the ionograms in the test database. For each epoch, the lowest difference in absolute value between the modelled MUF (IONORT-IRI-WC or IONORT-ISP-WC) and the measured MUF is highlighted in bold.

Epoch	A IONORT-IRI-WC MUF [MHz]	B IONORT-ISP-WC MUF [MHz]	C MEASURED MUF [MHz]	D Δ_{IRI} [MHz]	E Δ_{ISP} [MHz]
23 JUN 2011 – 17:00	13.7	11.5	10.7	3.0	**0.8**
23 JUN 2011 – 19:00	12.9	14.7	14.9	−2.0	**−0.2**
23 JUN 2011 – 23:00	10.0	8.3	8.6	1.4	**−0.3**
25 JUN 2011 – 10:00	14.6	14.5	13.4	1.2	**1.1**
25 JUN 2011 – 20:00	12.2	12.6	13.4	−1.2	**−0.8**
25 JUN 2011 – 23:00	9.9	11.2	11.4	−1.5	**−0.2**
26 JUN 2011 – 00:00	9.4	8.8	9.0	0.4	**−0.2**
26 JUN 2011 – 01:00	9.0	8.7	8.8	0.2	**−0.1**
26 JUN 2011 – 02:00	8.8	8.7	8.2	0.6	**0.5**
03 JUL 2011 – 17:00	13.6	15.1	15.1	−1.5	**0.0**
04 JUL 2011 – 19:00	12.9	13.5	13.8	−0.9	**−0.3**
04 JUL 2011 – 20:00	12.2	13.7	13.2	−1.0	**0.5**
06 JUL 2011 – 12:00	14.6	14.9	13.7	**0.9**	1.2
06 JUL 2011 – 21:00	11.6	12.4	13.5	−1.9	**−1.1**
07 JUL 2011 – 01:00	8.9	7.7	8.3	0.6	−0.6
07 JUL 2011 – 14:00	13.6	13.1	12.4	1.2	**0.7**
07 JUL 2011 – 15:00	13.5	13.3	13.0	0.5	**0.3**
07 JUL 2011 – 17:00	13.5	12.1	11.8	1.7	**0.3**
07 JUL 2011 – 18:00	13.2	12.9	13.5	**−0.3**	−0.6
07 JUL 2011 – 19:00	12.9	13.1	14.0	−1.1	**−0.9**
08 JUL 2011 – 17:00	13.5	12.1	12.1	1.4	**0.0**
08 JUL 2011 – 18:00	13.2	14.5	14.5	−1.3	**0.0**
08 JUL 2011 – 19:00	12.8	15.1	16.7	−3.9	**−1.6**
08 OCT 2011 – 06:15	14.8	16.4	15.9	−1.1	**0.5**
08 OCT 2011 – 06:45	14.7	18.0	17.7	−3.0	**0.3**
08 OCT 2011 – 10:30	19.3	16.4	20.5	**−1.2**	−4.1
08 OCT 2011 – 20:00	9.0	8.7	9.2	**−0.2**	−0.5
08 OCT 2011 – 23:45	7.6	6.8	7.7	**−0.1**	−0.9
09 OCT 2011 – 02:00	7.5	6.4	6.9	0.6	**−0.5**
09 OCT 2011 – 02:15	7.5	6.3	6.8	0.7	**−0.5**
09 OCT 2011 – 03:00	7.2	6.6	6.7	0.5	**−0.1**
09 OCT 2011 – 05:00	10.7	13.6	12.2	−1.5	**1.4**
09 OCT 2011 – 06:30	14.8	16.9	15.1	**−0.3**	1.8

absorption of the propagating wave through the ionosphere can be considered negligible because of the lack of the lower absorbing layers (D and E regions). For this reason, the LOF_F calculated with or without the electron collision frequency model for the D-layer show practically the same values. To better clarify this feature, we can refer to the legends of Fig. 4 where the LOF_F values are reported. For the epoch 9 October 2011 at 03:00 UT, both for IRI and ISP electron density profile grids (see second and third panel of Fig. 4 respectively), the LOF_F values calculated with or without the collisional model are equal to 3.0 MHz for 1-hop and 3-hop paths. The same occurs for the epoch 26 June 2011 at 01:00 UT where only very small differences are observed between the LOF_F calculated with NC and the LOF_F obtained in the case WC: discrepancies of 0.1 MHz (for 3-hop paths) and 0.4 MHz (for 1-hop paths) are observed when the IRI and ISP electron density profile grids are considered respectively, which means that during night-time the simulated ionograms do not show traces cut away at lower frequencies.

The results of this study are summarized in Table 1 where is shown the full database concerning the epochs for which the observed ionograms over the radio link Rome-Chania were selected according to the criteria (a) and (b) above mentioned.

The MUF calculated by both the IONORT-IRI-WC and the IONORT-ISP-WC system, and the measured MUF for all the ionograms of the test database, are shown together with the corresponding differences between the modelled (IONORT-IRI-WC or IONORT-ISP-WC system) and the measured MUF values. From the results shown in the columns D and E, it can be seen that IONORT-ISP-WC MUF values are close to the measured values in most of the cases considered.

To better highlight the results of Table 1, the results of the comparison between the differences (IONORT-IRI-WC MUF – measured MUF), and (IONORT-ISP-WC MUF – measured MUF), are also presented in Fig. 5 for the whole test database. It is clearly evident that IONORT-ISP-WC system performs better than IONORT-IRI-WC system

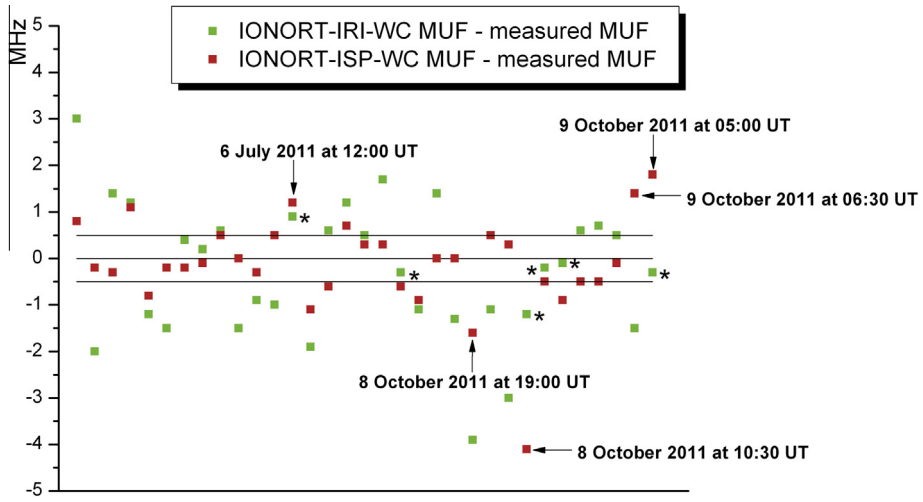

Fig. 5. Comparisons between the differences (IONORT-IRI-WC MUF – measured MUF) (green squares) and (IONORT-ISP-WC MUF – measured MUF) (red squares) for the whole test database. The arrows indicate the cases for which the IONORT-ISP-WC system mostly underestimates/overestimates the MUF values. The symbol * marks the 6 cases for which IONORT-IRI-WC system performs better than IONORT-ISP-WC system. (For interpretation of the references to colour in this figure legend, the reader is referred to the web version of this article.)

because in most of cases considered, the differences (IONORT-ISP-WC MUF – measured MUF) are very small (in particular, see in Fig. 5 the red squares ranged between the horizontal lines −0.5 – 0.5 MHz), and only in six cases (see in Fig. 5 the green squares marked with the symbol *) is the performance of IONORT-IRI-WC better than that of IONORT-ISP-WC.

4. Conclusions and future developments

The oblique ionograms synthesized by the IONORT-ISP-WC system are generally better than the oblique ionograms synthesized by the IONORT-IRI-WC system. From the analysis conducted on the whole database, it emerges that the IONORT-ISP-WC MUF values are more accurate than the IONORT-IRI-WC MUF values (see Table 1 and Fig. 5). As expected, this means that the representation of the ionosphere produced by the ISP model is more realistic than the climatological representation produced by the IRI model, and also that the ray-tracing results performed by the IONORT algorithm are reasonably reliable.

Nevertheless, Table 1 and Fig. 5 show also some cases for which the MUF values provided by the IONORT-ISP-WC system are greatly underestimated, on 8 October 2011 at 19:00 UT and, most noticeably, on 8 October 2011 at 10.30 UT, or overestimated, on 6 July 2011 at 12:00 UT, and 9 October 2011 at 05:00 and 06:30 UT. In these cases no data was available from Rome and Gibilmanna, and the only reference ionospheric station contributing to the ISP grids was Athens. This estimate of MUF values provided by the IONORT-ISP-WC system could probably be smoothed out by including additional ionospheric reference stations in the region of interest, and especially located around the midpoint of the path considered.

It is also worth noting that the comparison of the synthesized ionograms with or without the collisional model used in this study (see for example Figs. 3 and 4), shows that during daytime, for the lower ionospheric layers, the traces of the synthesized ionograms are cut away at low frequencies; during night-time, when the lower ionospheric layer are missing and the absorption is not important, the traces of the simulated ionograms for the higher ionospheric layers are not cut off at low frequencies. These results provide a further confirmation about the goodness of the IONORT-ISP-WC system in providing consistent results.

In summary, the results presented in this paper suggest that: (a) the assimilation of data measured at multiple ionospheric reference stations by ISP is very important to obtain as reliable an image of the ionosphere as possible; (b) the IONORT-ISP-WC system can be proposed as a valid tool for operational use.

With regard to future developments, the IONORT-ISP-WC system does not provide a procedure to compute the horizontal gradients of the ionosphere, although the electron density profile grids are now characterized by a denser resolution in the latitude and longitude coordinates, i.e. from $2° \times 2°$ to $1° \times 1°$. This issue will be addressed in the future by developing a procedure capable of taking the presence of horizontal gradients into account, in order to improve the IONORT-ISP-WC system.

Moreover, more oblique sounding measurements will need to be conducted in order to investigate the issue of the underestimates/overestimates of MUF values and further test the behaviour of the IONORT-ISP-WC system.

Acknowledgments

The authors are extremely grateful to Dr. Bruno Zolesi and Dr. Ljiljana Cander for the useful simulations generated by the SIRMUP model; Dr. Carlo Scotto for interesting pointers to literature regarding ionospheric models and

ray-tracing; Dr. Enrico Zuccheretti, and Prof. J. Makris for their helpful discussions regarding oblique ionograms; and Dr. Alessandro Pignatelli for his valuable computer support.

References

Angling, M.J., Jackson-Booth, N.K., 2011. A short note on the assimilation of collocated and concurrent GPS and ionosonde data into the electron density assimilative model. Radio Sci. 46 (6), RS0D13. http://dx.doi.org/10.1029/2010RS004566.

Angling, M.J., Khattatov, B., 2006. Comparative study of two assimilative models of the ionosphere. Radio Sci. 41 (5), RS5S20. http://dx.doi.org/10.1029/2005RS003372.

Appleton, E.V., Chapman, F.W., 1932. The collisional friction experienced by vibrating electrons in ionized air. Proc. Phys. Soc. London 44 (3), 246–254. http://dx.doi.org/10.1088/0959-5309/44/3/302.

Azzarone, A., Bianchi, C., Pezzopane, M., Pietrella, M., Scotto, C., Settimi, A., 2012. IONORT: a Windows software tool to calculate the HF ray tracing in the ionosphere. Comput. Geosci. 42, 57–63. http://dx.doi.org/10.1016/j.cageo.2012.02.008.

Bianchi, C., Settimi, A., Scotto, C., Azzarone, A., Lozito, A., 2011. A method to test HF ray tracing algorithm in the ionosphere by means of the virtual time delay. Adv. Space Res. 48 (10), 1600–1605. http://dx.doi.org/10.1016/j.asr.2011.07.020.

Budden, K.G., 1965. Effect of electron collisions on the formulas of magnetoionic theory. Radio Sci. 69D (2), 191–211.

Coleman, C.J., 1998. A ray-tracing formulation and its application to some problems in over-the-horizon radar. Radio Sci. 33 (4), 1187–1197. http://dx.doi.org/10.1029/98RS01523.

Croft, T.A., Gregory, L., 1963. Stanford University, Stanford Electronics Laboratories, Fast, versatile ray-tracing program for IBM 7090 digital computers, Defense Technical Information Center (ed.), Rept. SEL-63-107, TR 82, Contract No. 225 (64), Office of Naval Research, Advanced Research Projects Agency, Stanford, California, USA, 28 p.

Davies, K., 1990. Ionospheric Radio, Peter Peregrinus Ltd. (ed.) on behalf of the Institution of Electrical Engineers (IET), London, UK, 508 p.

Decker, D.T., McNamara, L.F., 2007. Validation of ionospheric weather predicted by global assimilation of ionospheric measurements (GAIM) models. Radio Sci. 42 (4), RS4017. http://dx.doi.org/10.1029/2007RS003632.

Dudziak, W.F., 1961. Three-dimensional ray trace computer program for electromagnetic wave propagation studies, Technical Military Planning Operation RM 61TMP-32, Defense Atomic Support Agency DASA 1232, General Electrical Company, Santa Barbara, California, USA, 170 p.

Fridman, S.V., Nickisch, L.J., Aiello, M., Hausman, M., 2006. Real-time reconstruction of the three-dimensional ionosphere using data from a network of GPS receivers. Radio Sci. 41 (5), RS5S12. http://dx.doi.org/10.1029/2005RS003341.

Fridman, S.V., Nickisch, L.J., Hausman, M., 2009. Personal-computer-based system for real-time reconstruction of the three-dimensional ionosphere using data from diverse sources. Radio Sci. 44 (3), RS3008. http://dx.doi.org/10.1029/2008RS004040.

Haselgrove, J., 1955. Ray theory and a new method of ray tracing. In: Conference on the Physics of the Ionosphere, Proc. Phys. Soc. London, vol. 23, pp. 355–364.

Haselgrove, C.B., Haselgrove, J., 1960. Twisted ray paths in the ionosphere. Proc. Phys. Soc. London 75 (3), 357–363. http://dx.doi.org/10.1088/0370-1328/75/3/304.

Jones, R.M., 1966. A three dimensional ray tracing computer program, ESSA Tech. Rep., IER 17-ITSA 17, Government Printing Office, Washington, USA.

Jones, R.M., Stephenson, J. J., 1975. A versatile three-dimensional ray tracing computer program for radio waves in the ionosphere, OT Report, 75–76, U.S. Department of Commerce, Office of Telecommunication, U.S. Government Printing Office, Washington, USA, 185 p.

Kashcheyev, A., Nava, B., Radicella, S.M., 2012. Estimation of higher-order ionospheric errors in GNSS positioning using a realistic 3-D electron density model. Radio Sci. 47 (4), RS4008. http://dx.doi.org/10.1029/2011RS004976.

Lawrence, R.S., Posakony, D.J., 1961. A digital ray tracing program for ionospheric research. In: van de Hulst, H.C., de Jager, C., Moore, A.F. (Eds.), Proc. Intern. Space Sci. Symp., vol. 2. North Holland, Amsterdam, pp. 258–276.

McNamara, L.F., 1991. The Ionosphere: Communications, Surveillance, and Direction Finding (Orbit: A Foundation Series). Krieger Pub Co (Hardcover, 248 p.).

McNamara, L.F., Decker, D.T., Welsh, J.A., Cole, D.G., 2007. Validation of the Utah state university global assimilation of ionospheric measurements (GAIM) model predictions of the maximum usable frequency for a 3000 km circuit. Radio Sci. 42 (3), RS3015. http://dx.doi.org/10.1029/2006RS003589.

McNamara, L.F., Baker, C.R., Decker, D.T., 2008. Accuracy of USU-GAIM specifications of foF2 and M(3000)F2 for a worldwide distribution of ionosonde locations. Radio Sci. 43 (1), RS1011. http://dx.doi.org/10.1029/2007RS003754.

McNamara, L.F., Retterer, J.M., Baker, C.R., Bishop, G.J., Cooke, D.L., Roth, C.J., Welsh, J.A., 2010. Longitudinal structure in the CHAMP electron densities and their implications for global ionospheric modelling. Radio Sci. 45 (2), RS2001. http://dx.doi.org/10.1029/2009RS004251.

McNamara, L.F., Bishop, G.J., Welsh, J.A., 2011. Assimilation of ionosonde profiles into a global ionospheric model. Radio Sci. 46 (2), RS2006. http://dx.doi.org/10.1029/2010RS004457.

McNamara, L.F., Angling, M.J., Elvidge, S., Fridman, S.V., Hausman, M.A., Nickisch, L.J., McKinnell, L.-A., 2013. Assimilation procedures for updating ionospheric profiles below the F2 peak. Radio Sci. 48 (2), 143–157. http://dx.doi.org/10.1002/rds.20020.

Nickisch, L.J., 2008. Practical applications of Haselgrove's equations for HF systems. Radio Sci. Bull. 325, 36–48, http://www.ursi.org/files/RSBissues/RSB_325_2008_06.pdf.

Norman, R.J., Cannon, P.S., 1997. A two-dimensional analytic ray tracing technique accommodating horizontal gradients. Radio Sci. 32 (2), 387–396. http://dx.doi.org/10.1029/96RS03200.

Pezzopane, M., Pietrella, M., Pignatelli, A., Zolesi, B., Cander, L.R., 2011. Assimilation of autoscaled data and regional and local ionospheric models as input sources for real-time 3-D International Reference Ionosphere modelling. Radio Sci. 46 (5), RS5009. http://dx.doi.org/10.1029/2011RS004697.

Pezzopane, M., Pietrella, M., Pignatelli, A., Zolesi, B., Cander, L.R., 2013. Testing the three-dimensional IRI-SIRMUP-P mapping of the ionosphere for disturbed periods. Adv. Space Res. 52 (10), 1726–1736. http://dx.doi.org/10.1016/j.asr.2012.11.028.

Rawer, K., 1976. Manual on ionospheric absorption measurements. In: Raver, K. (Ed.), World Data Center A for Solar-Terrestrial Physics. NOAA, Boulder, Colorado, USA (and printed by U.S. Department of Commerce National Oceanic and Atmospheric Administration Environmental Data Service, Asheville, Noth Carolina, USA, 202 p.).

Sen, H.K., Wyller, A.A., 1960. On the generalization of the appleton–hartree magnetoionic formulas. J. Geophys. Res. 65 (12), 3931–3950. http://dx.doi.org/10.1029/JZ065i012p03931.

Settimi, A., Pezzopane, M., Pietrella, M., Bianchi, C., Scotto, C., Zuccheretti, E., Makris, J., 2013. Testing the IONORT-ISP system: a comparison between synthesized and measured oblique ionograms. Radio Sci. 48 (2), 167–179. http://dx.doi.org/10.1002/rds.20018.

Settimi, A., Pietrella, M., Pezzopane, M., Zolesi, B., Bianchi, C., Scotto, C., 2014. The COMPLEIK subroutine of the IONORT-ISP system for calculating the non-deviative absorption: A comparison with the ICEPAC formula. Adv. Space. Res. 53 (2), 201–218. http://dx.doi.org/10.1016/j.asr.2013.10.035.

Shim, J.S., Kuznetsova, M., Rastätter, L., et al., 2011. CEDAR electrodynamics thermosphere ionosphere (ETI) challenge for systematic assessment of ionosphere/thermosphere models: NmF2, hmF2,

and vertical drift using ground-based observations. Space Weather 9 (12), S12003. http://dx.doi.org/10.1029/2011SW000727.

Stewart, F. G., Ionospheric Communications Enhanced Profile Analysis & Circuit (ICEPAC) Prediction Program, Technical Manual, 91 pp., undated. (http://elbert.its.bldrdoc.gov/hf_prop/manuals/icepac_tech_manual.pdf).

Thompson, D.C., Scherliess, L., Sojka, J.J., Schunk, R.W., 2006. The Utah State University Gauss–Markov Kalman filter of the ionosphere: the effect of slant TEC and electron density profile data on model fidelity. J. Atmos. Solar-Terr. Phys. 68 (9), 947–958. http://dx.doi.org/10.1016/j.jastp.2005.10.011.